Electronic Supplementary Material (ESI) for Journal of Materials Chemistry C.


# $Cs_2AgBiBr_{6-x}Cl_x$ solid solutions – Band gap engineering with halide double perovskites

Matthew B. Gray, Eric T. McClure, and Patrick M. Woodward

## Supporting Information

### Figures:

**Fig. S1** - Rietveld refined PXRD pattern of $Cs_2AgBiBr_3Cl_3$ in the $Fm\bar{3}m$ space group, tick marks signify the positions of the allowed *hkl* reflections.

**Fig. S2** Diffuse reflectance spectroscopy (DRS) data for the solid solution series, $Cs_2AgBiBr_{6-x}Cl_x$.

**Fig. S3** Energy of the direct $Bi^{3+}$ $6s^2 \rightarrow 6s^16p^1$ transition absorption maximum, obtained from the Kubelka-Munk (KM) transformation of the DRS data as a function of chloride content.

### Tables:

**Table S1** Gaussian microstrain broadening for $Cs_2AgBiBr_{6-x}Cl_x$ samples as a function of the $Cl^-$ content, and goodness of fit parameters from Rietveld refinements with and without strain, and crystallite size broadening.

**Table S2** Comparison of nominal $Cl^-$ content and occupational and thermal values obtained from refinement of the anion site occupancies obtained from Rietveld refinements.

**Table S3** Energies of the indirect band gap and absorption maximum of the localized $Bi^{3+}$ $6s^2 \rightarrow 6s^16p^1$ transition as a function of $Cl^-$ content in $Cs_2AgBiBr_{6-x}Br_x$ samples.

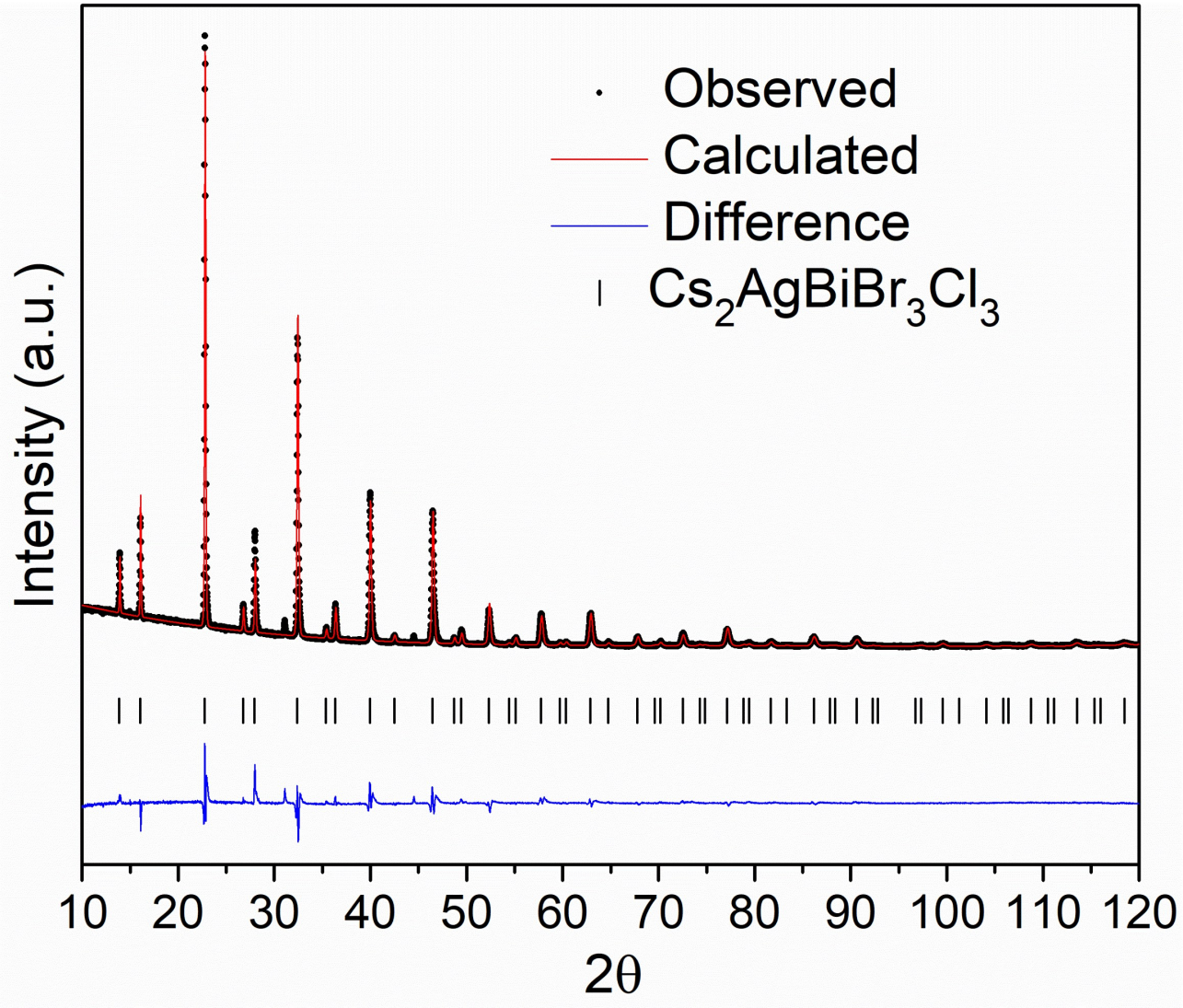


**Fig. S1** Rietveld refined PXRD pattern of $Cs_2AgBiBr_3Cl_3$ in the $Fm\bar{3}m$ space group, tick marks signify the positions of the allowed *hkl* reflections.

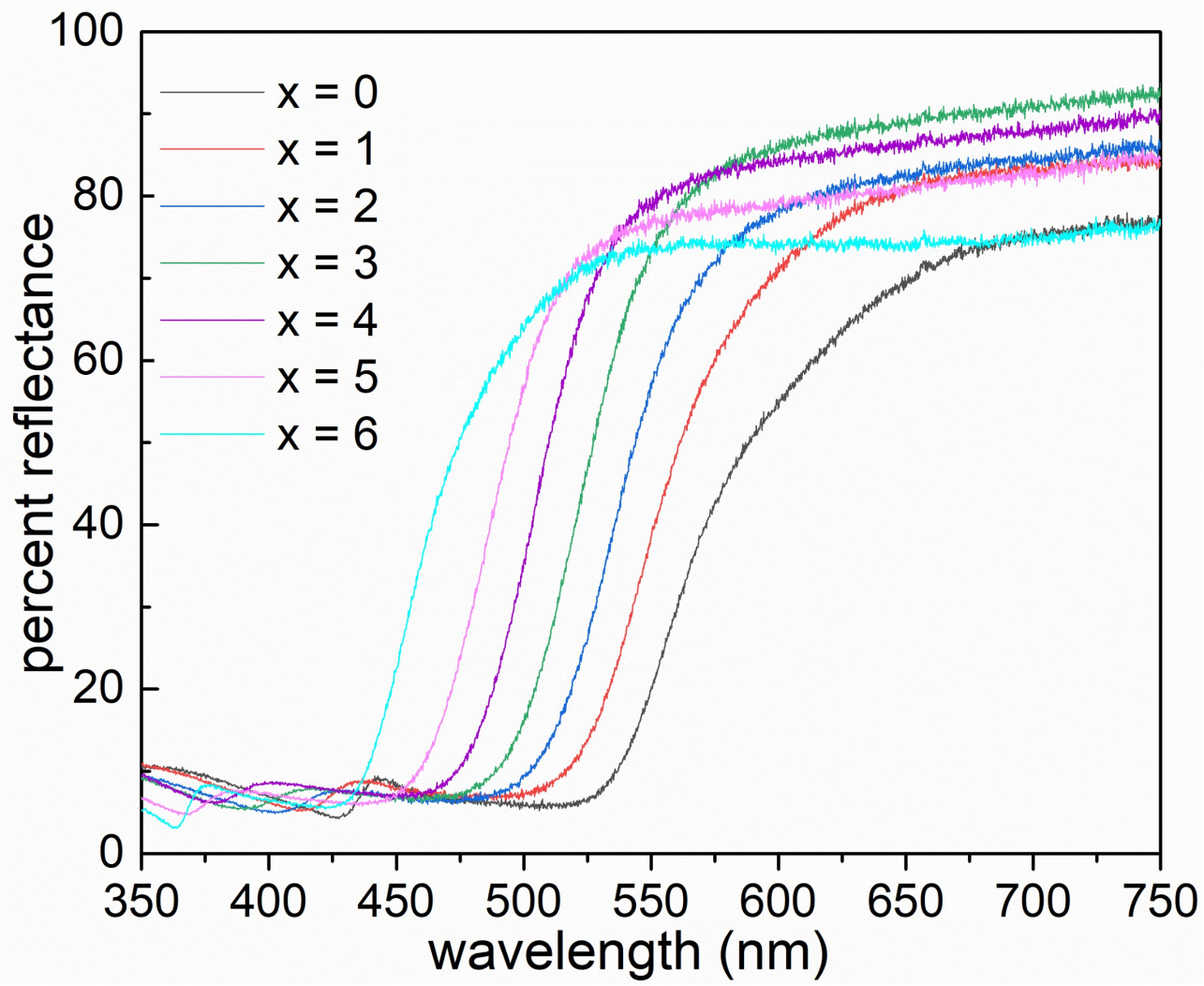


**Fig. S2** Diffuse reflectance spectroscopy (DRS) data for the solid solution series, $Cs_2AgBiBr_{6-x}Cl_x$.

**Table S1** Gaussian microstrain broadening for $Cs_2AgBiBr_{6-x}Cl_x$ samples as a function of the $Cl^-$ content, and goodness of fit parameters from Rietveld refinements with and without strain and crystallite size broadening.

| | **x = 0** | **x = 1** | **x = 2** | **x = 3** | **x = 4** | **x = 5** | **x = 6** |
|---|---|---|---|---|---|---|---|
| Gaussian microstrain | 0.004(3) | 0.128(3) | 0.301(5) | 0.502(4) | 0.612(3) | 0.701(2) | 0.067(1) |
| $R_{wp}$ no strain | 6.473 | 21.884 | 30.363 | 32.092 | 32.078 | 35.982 | 11.952 |
| $R_{wp}$ strain | 6.475 | 17.086 | 17.632 | 10.688 | 8.208 | 7.476 | 6.024 |
| $R_{wp}$ strain and size | 6.524 | 17.092 | 17.619 | 10.669 | 8.017 | 7.441 | 6.057 |

Strain analysis was conducted using the Rietveld method, within TOPAS-Academic (Version 6). To account for instrumental broadening, the $Cs_2AgBiBr_6$ end-member was fit (this sample had the sharpest peaks). The values for the axial term, "Simple_Axial_Model" and the TCHZ peak shape parameters of the remaining samples were fixed at the values obtained for the $Cs_2AgBiBr_6$ refinement. Initial Rietveld refinements were conducted, using locked occupancies, atomic positions, and sample height from the freely refined analysis of the solid solutions. These $R_{wp}$ values are reported in Table S1, in the "$R_{wp}$ no strain" row. Then, the strain macros, "e0_from_Strain," was added to the refinement to determine the amount of Gaussian and Lorentzian strain in the system. These $R_{wp}$ values are reported in Table S1, in the "$R_{wp}$ strain" row. In all cases, the Gaussian strain was at least an of magnitude larger than the Lorentzian strain; therefore, it was determined that microstrain caused by localized anion disorder was the primary cause of peak broadening.[2] The final row of Table S1 gives the $R_{wp}$ values obtained when both Gaussian strain and crystallite size effects were used to model the peak shapes. The similarity of the last two rows of Table S1 shows that the broadening due to crystallite size effects is minimal and can be neglected.

The occupancy of the anion site was refined in all samples, with the restraint that the $Cl^-$ + $Br^-$ occupancy adds up to 1. The results are given in Table S2. In general, the refined occupancies were with a few percent of the nominal occupancies.

**Table S2** Comparison of nominal $Cl^-$ content and values obtained from refinement of the anion site occupancies obtained from Rietveld refinements.

| **Nominal Percent Cl** | **Refined Percent Cl** | **Halide $B_{eq}$** |
|---|---|---|
| 0 % | 0.0(2) % | 3.45(4) |
| 16.7 % | 17(1) % | 3.81(7) |
| 33.3 % | 31(1) % | 3.43(9) |
| 50.0 % | 53.5(7) % | 3.69(6) |
| 66.7 % | 70.6(5) % | 3.51(7) |
| 83.3 % | 87.7(5) % | 3.60(4) |
| 100 % | 100.0(4) % | 3.47(4) |

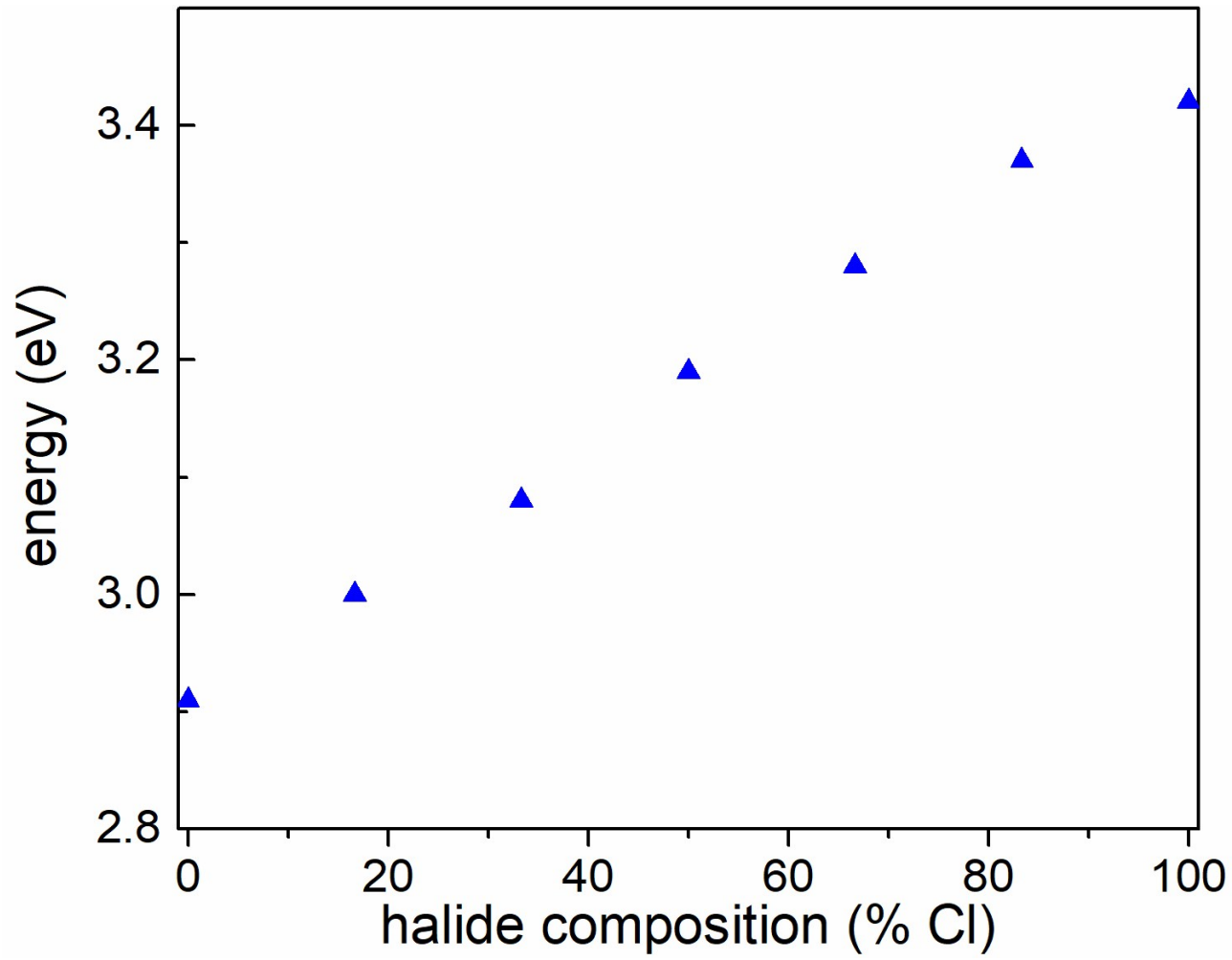


**Fig. S3** Energy of the direct $Bi^{3+}$ $6s^2 \rightarrow 6s^16p^1$ transition absorption maximum, obtained from the Kubelka-Munk (KM) transformation of the DRS data as a function of chloride content. Error bars are smaller than the symbols used to plot the data.

**Table S3** Energies of the indirect band gap and absorption maximum of the localized $Bi^{3+}$ $6s^2 \rightarrow 6s^16p^1$ transition as a function of $Cl^-$ content in $Cs_2AgBiBr_{6-x}Br_x$ samples.

| Nominal Percent Cl | Band Gap (eV) | Local $6s^2 \rightarrow 6s^16p^1$ (eV) |
|---|---|---|
| 0.00 % | 2.20(1) | 2.91(2) |
| 16.67 % | 2.27(2) | 3.00(1) |
| 33.33 % | 2.34(1) | 3.08(1) |
| 50.00 % | 2.41(1) | 3.19(1) |
| 66.67 % | 2.51(1) | 3.28(2) |
| 83.33 % | 2.60(2) | 3.37(1) |
| 100.00 % | 2.77(1) | 3.42(1) |

## References


1. Topas-Academic (Version 6), General Profile and Structural Analysis for Powder Diffraction Data; Bruker AXS: Karlsruhe, Germany, 2004.

2. Balzar *et. al.*, *J. Appl. Cryst*. 2004, **37**, 911.